Wind Energ. Sci., 11, 2037–2051, 2026
https://doi.org/10.5194/wes-11-2037-2026

eawe european academy of wind energy
Open Access WIND ENERGY SCIENCE

Experimental validation and extension of a blade element momentum model for counter-rotation dual-rotor wind turbine with double rotational armature design

Niels Cornelis Adema[1], Josep Gil-Vernet Pagonabarraga[1,2], Wouter Swart Ranshuysen[2], Arjen de Ruijter[2], and Gerard Schepers[1,3]

[1]Entrance – Centre of Expertise Energy part of Hanze UAS, Groningen, 9747AA, the Netherlands
[2]Institute of Engineering, section Mechanical Engineering, Hanze UAS, Groningen, 9747AS, the Netherlands
[3]TNO Energy Transition and Materials, 2628 CK, Delft, the Netherlands

Correspondence: Niels Cornelis Adema (ni.c.adema@pl.hanze.nl)

Received: 9 November 2025 – Discussion started: 19 November 2025
Revised: 18 April 2026 – Accepted: 25 May 2026 – Published: 10 June 2026

Abstract. Small wind turbines face significant challenges in achieving commercial viability due to lower efficiency and higher energy costs compared to utility-scale systems and competing renewable technologies. Counter-rotating dual-rotor wind turbines (CR-DRWTs) with dual-rotational armature configurations offer a potential pathway for efficiency improvements through doubled direct-drive power and minimal mechanical complexity, suitable for urban applications. This study presents a detailed experimental investigation of a 1.6 m diameter CR-DRWT through wind tunnel testing at the Centre Scientifique et Technique du Bâtiment (CSTB) in Nantes, France, conducted at wind speeds between 4 and 15 m s^{-1}. An improved turbine design is tested with enhanced instrumentation, including independent measurements of rotor rotational speed and blade pitch angle, enabling a detailed characterization of rotor interaction, operating behaviour, and power performance. The turbine achieved a maximum electrical power output of 1014 W and a peak measured power coefficient of 0.33 while demonstrating reliable self-starting at wind speeds as low as 3.5 m s^{-1}. To interpret and generalize the experimental findings, an existing blade element momentum (BEM) model for dual-rotor systems is extended to explicitly represent torque balance and power production in a dual-rotational armature configuration. The extended model shows good agreement with experimental trends and is further applied in a sweep optimization. The optimized configuration predicts a theoretical maximum power coefficient of 0.56, highlighting substantial remaining performance potential. By combining wind tunnel measurements with a validated BEM model extension, this work provides unique reference data and supports the development of mechanically simple CR-DRWTs for future small-scale wind energy systems.

1 Introduction

While modern wind turbines have become the largest rotating machines on earth with further upscaling planned, renewed interest in small wind turbines (SWTs) is fostered through local energy transition and smart grid development. SWTs have traditionally lacked the aerodynamic refinement of larger turbines, resulting in lower efficiency, lower capacity factors, and higher energy costs (Bianchini et al., 2022). Still, SWTs serve diverse applications worldwide, including power generation for households, industrial centres, farms, and isolated communities; hybrid energy systems for remote monitoring and telecommunications; and direct energy services like water pumping, desalination, and purification (Chagas et al., 2020). While SWTs can outperform photovoltaic (PV) systems in annual power generation at specific locations, investments require site-specific wind resource assessments, and support schemes must avoid subsidizing low-potential areas (Jurasz et al., 2025). Studies have also shown potential for urban wind applications (Bereziartua-Gonzalez et al.,

2025; Calautit and Johnstone, 2023). Despite these opportunities, SWTs face significant economic challenges. Their energy costs typically exceed both residential electricity prices and those of competing technologies like rooftop solar and utility-scale wind farms. These elevated costs stem from limited development compared to large-scale systems, as well as disproportionately high expenses for electrical connection, resource assessment, and installation (Simic et al., 2013). To achieve commercial viability, SWTs must either achieve substantial cost reductions, for example, through targeted policy incentives (Jurasz et al., 2025), or must significantly improve their energy capture capability (Bianchini et al., 2022).

Dual-rotor wind turbine (DRWT) configurations represent one potential pathway for efficiency gains, though this approach introduces trade-offs such as higher manufacturing costs, increased structural weight, and greater mechanical complexity. DRWTs can be categorized into co-rotating systems (CO-DRWTs), where both rotors rotate in the same clockwise direction, or counter-rotating systems (CR-DRWTs) where one rotor rotates clockwise and the other counter-clockwise. Several mechanical configurations exist for dual-rotor wind turbines (DRWTs). Multiple experiments are performed on individual wind turbines placed close together or a set-up with two rotors, each with a separate generator. To design a complete single DRWT system, one approach employs a bevel gear system that connects both rotors to a single generator shaft (Jung et al., 2005; Schepers et al., 2024). Alternatively, a double rotational armature generator features one rotor connected to the generator stator and the other to the generator rotor (Adema et al., 2025; Booker et al., 2010; Mitulet et al., 2015). This latter configuration offers notable advantages, including doubled direct-drive power, minimal starting torque, high electrical and mechanical efficiency, compact design, and reduced noise and vibration – characteristics that make it particularly suitable for small-scale urban wind applications.

Newman (1986) extended the classical 1D Betz theory for single-actuator discs to configurations with multiple discs, demonstrating that a dual-rotor system can theoretically achieve a power coefficient (CP) of $8/75 = 0.64$, with an induction factor of $3/5$ at the second rotor. These values exceed those of a single rotor operating at the Betz limit ($\mathrm{CP} = 0.59$, induction factor $= 1/3$). Through smoke visualization experiments in a wind tunnel using porous discs at varying separation distances, Newman recommended a minimum spacing of $0.5\,D$ (where D is the rotor diameter) between discs to minimize flow curvature and non-uniformity, thereby maintaining the validity of the 1D assumptions. More recently, Sundararaju et al. (2017) investigated CR-DRWTs with equal-diameter rotors. They found that the maximum achievable CP reaches 0.814 when the rotors are separated by an axial distance of $2.8\,D$. Their work also revealed that reducing the axial spacing toward zero causes the power coefficient to decrease progressively toward the single-rotor Betz limit.

A limited amount of field- and lab-scale testing on DRWTs has been performed in the last few years. A field test by Jung et al. (2005) showed a CP of approximately 0.5 for a 30 kW CR-DRWT with asymmetric rotors (5.5 m front, 11 m rear) connected via bevel gears to a planetary gearbox, with simulations indicating optimal performance at $0.5\,D$ spacing. Small-scale wind tunnel experiments on DRWTs are more common and have produced varying results. Habash et al. (2011) and Mitulet et al. (2015) both reported approximately 60 % increases in energy production compared to single-rotor configurations, testing turbines with rotor diameters of 23 cm and 2.5 m, respectively, at spacings ranging from 0.3 to 2.3 and $0.4\,D$. The first used an individual generator per rotor, and the latter used a double-rotational armature configuration. Zhao et al. (2020) found relative improvements in the CP of 5.3 %–28.9 % with a 0.55 m radius turbine at optimal $0.3\,D$ spacing and individual generators per rotor. The CP values found were 0.34–0.41 versus 0.31–0.35 for single-rotor operation at 8–14 $\mathrm{m\,s^{-1}}$ wind speed. A wind tunnel test including particle image velocimetry (PIV) measurements comparing co- and counter-rotating DRWT systems conducted by Ozbay et al. (2014) found a 60 % power increase for a counter-rotating DRWT and a 48 % increase for a co-rotating DRWT compared to a single-rotor configuration. Individual turbine models with 1.27 m radius at different spacings (0.7–6.5 D) were tested by Yuan et al. (2014). It was found that counter-rotating produced 20 % more power compared to co-rotating in the near wake, which decreased to only 4 % at $5.0\,D$. Wang et al. (2018) tested asymmetric rotor designs (0.28 m front, 0.15 m rear, with $0.25\,D$ spacing) and observed smaller gains of 7.2 % for counter-rotating and 1.8 % for co-rotating configurations. At $3.5\,D$, Mühle et al. (2017) found a significant improvement of 2 % in power production by operating the upstream rotor counter rotating.

On the contrary, no power increase was found for a bevel gear CR-DRWT system with 1.6 m rotors at $0.64\,D$ spacing by Schepers et al. (2024). However, more recently, Adema et al. (2025) tested the same turbine with a double-rotational armature design instead of bevel gears and observed a 10 % CP increase, highlighting how mechanical and electrical design may influence the observed performance of DRWT systems.

Modelling of DRWT systems can be categorized in two primary approaches. Blade element momentum (BEM) and computational fluid dynamics (CFD) offer complementary insights into DRWT performance with the BEM method commonly used as the preferred tool (Peng et al., 2025). Several BEM models have been developed for DRWT systems. Lee et al. (2012) proposed a modified BEM model for CR-DRWTs in which the rear rotor operates in the fully developed wake of the front rotor, prescribing the axial velocity deficit and neglecting tangential effects and downstream-to-upstream interactions. Yin et al. (2022) improved physical fidelity by coupling a BE/M–T model with free-wake lifting-line data, capturing both axial and tangential inter-rotor velocity interferences, albeit with increased modelling com-

plexity. Amoretti et al. (2023) instead developed a configurable BEM-based approach that retains the dominant upstream wake effects while deliberately neglecting rear-to-front feedback. This offers a robust and computationally efficient framework that is particularly well suited for CR-DRWT performance prediction and parametric design studies and that will be used in this study. Experimental validation is crucial to increase the accuracy of these methods. Both Amoretti et al. (2023) and Yin et al. (2022) developed BEM models dedicated to DRWT systems, with the first finding an increase in CP of 10.6 % for a CR-DRWT with respect to a single rotor and with the latter finding a 5 % CP increase. Additionally, several studies modelled DRWT systems using CFD simulations. Wang et al. (2022) modelled a diverse range of DRWT systems using CFD-RANS (co- and counter-rotating rotors of varied sizes, including configurations with equally but also non-equally sized rotors). Compared to single-rotor systems, an increase in performance is found for all configurations. The benefit in terms of performance in a counter-rotating system compared to in a co-rotating system is less conclusive. A net benefit of 7 % CP is found by Rosenberg et al. (2014) using RANS by modelling the NREL 5 MW rotor in combination with a 25 % size secondary rotor at 0.2 D and a 4.6 % benefit using large-eddy simulations. Another CFD simulation on the NREL 5 MW rotor with an additional rotor of 180 kW at 0.1 D downstream of the main rotor resulted in additional performance of 1.74 % despite both rotors having slight efficiency decreases (Peng et al., 2025). For equal-sized rotors at 0.5 D spacing, a peak CP of 0.53 is found by Koehuan et al. (2017) using CFD simulations.

The modelling of DRWT systems has furthermore received growing attention as a means to interpret experiments and to explore operational parameters. Building on the work of Amoretti et al. (2023), the present study adopts and extends their model to represent a counter-rotating DRWT equipped with a double-rotational armature generator, using experimental data as the primary reference for validation and model refinement. The core contribution of this study lies in the presentation and analysis of experimental wind tunnel measurements obtained from a counter-rotating dual-rotor wind turbine tested at the Centre Scientifique et Technique du Bâtiment (CSTB) in Nantes, France, within the framework of the 2025 International Small Wind Turbine Competition. The tested turbine represents an improved design iteration of the system presented by Adema et al. (2025) and incorporates additional instrumentation, including independent rotational speed and pitch measurements for both rotors. These measurements enable a more detailed characterization of rotor interactions, operating conditions, and power performance that has, so far, been scarcely documented for CR-DRWTs with double-rotational armature design. In addition to reporting experimental results, the study employs an extended BEM model to interpret the measurements and to perform an operation optimization of the pitch angle settings and the design tip speed ratios. By grounding the modelling and optimization directly in experimental evidence, this work provides new reference data and valuable insights that support the future development and optimization of compact counter-rotating wind turbines for small-scale applications.

The remainder of the paper is structured as follows: Sect. 2.1 presents the design of the CR-DRWT, after which the wind tunnel set-up and procedure are explained in Sect. 2.2. The BEM model, as well as adaptations for a double-rotational armature design, is shown in Sect. 2.3. An optimization algorithm for operational parameters is laid out in Sect. 2.4. The results of the wind tunnel test, BEM model, and optimization are shown in Sect. 3, after which the results are discussed in Sect. 4. Conclusions are presented in Sect. 5.

2 Methods and materials

This chapter describes the method and materials used in the study. The mechanical, electrical, and aerodynamic designs of the CR-DRWT are presented, after which the test procedure in the wind tunnel is explained. The BEM model used is explained, including proposed extensions to model a dual-rotational armature design. Finally, an optimization strategy is presented to determine optimal operating conditions for future designs.

2.1 Design of the CR-DRWT

The mechanical, electrical, and aerodynamic designs of the CR-DRWT used in this study are presented in earlier work for a different wind tunnel (Adema et al., 2025). The mechanical and electrical designs of the current turbine are identical to those in the earlier work. The generator is still an inline Windstream 1.4 kW permanent magnet direct current (PMDC) with the following operating conditions: 0–120 V, maximum current of 20 A for 30 min, 10 A continuous operation, and startup torque of 0.153 Nm. The overall efficiency of the generator under the contest conditions has been determined in previous work to be 70 %–90 % (Adema et al., 2025; Jansma, 2024). An overview of the mechanical design, including the blade pitching mechanism and blade mounts, is shown in Fig. 1. Some significant changes have been made to the aerodynamic design, as well as to the sensors on the turbine.

Numerous studies emphasize the importance of measuring blade pitch angles and rotor RPM during wind tunnel measurements of wind turbines (Adema et al., 2025; Amoretti et al., 2023; Bai et al., 2023; Bontempo and Manna, 2025; Erturk et al., 2018; Zhao et al., 2020). Thereto, additional sensors measuring RPM and pitch angles are mounted on the CR-DRWT. Rotor RPM is measured with light pulses passing through slotted discs connected to the rotor and stator and measured by two calibrated light gate sensors. During testing, only the upstream rotor RPM measurement was functional. Pitch angles are set with four Actuonix Motion P16-R

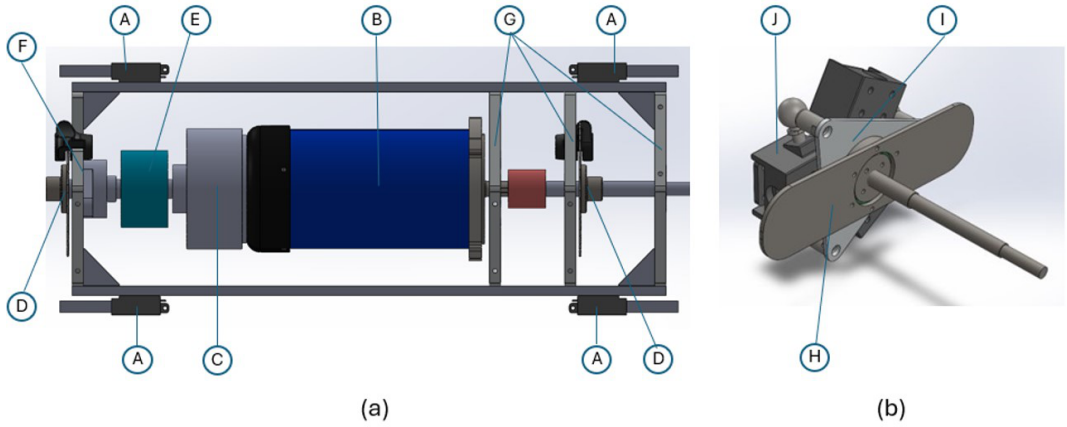

Figure 1. Overview of the mechanical lay-out of the CR-DRWT. **(a)** Nacelle overview, **(b)** pitch mechanism (in which A is the linear actuators, B is the generator, C is the generator cap, D is the disc brakes, E is the slip ring, F is the plate with external bearing, G shows the plates with internal bearing, H is the push–pull plate, I is the triangular place, and J shows the blade holders.). Taken from Adema et al. (2025).

linear actuators controlled by an Arduino Mega board with two L298B motor drivers. An Arduino-based control system is used to operate pitch and brake actuators, while the generator output is monitored in real time through a Python-based data acquisition interface.

The initial pitch angle for the mounting system for the blades is changed slightly, and, therefore, the twist distribution at zero pitch changes. The corresponding chord and twist distribution are shown in Fig. 2 alongside a zoom-in of the root section of the blade and connection to the blade holders. The blades consist of SG6043 airfoils and are fabricated with a 3D-printed core laminated with two carbon fibre layers. For simplicity, the downstream rotor is mirrored with respect to the upstream rotor. The distance between rotors is fixed at 0.64 m (0.39 D) for this CR-DRWT. The rotor diameter for both rotors is 1.6 m, leading to a 2 m^2 swept frontal area.

2.2 Wind tunnel set-up and test procedure

The CR-DRWT is tested in the aerodynamic test section at CSTB. The section is 12 m long and 6 m wide and has a height of 5 m. The airflow is controlled to keep a uniform and constant velocity, taking into consideration air density variations. The maximum free-stream wind speed is 70 $m\,s^{-1}$. Turbulence intensity in the empty test section is less than 1.5 % (Braud et al., 2024). The blockage ratio of the 2 m^2 rotor is 6.7 %, which is below the 10 % mentioned in the literature, above which corrections need to be made (Al-Obaidi and Madivaanan, 2022; Chen and Liou, 2011; Jeong et al., 2018).

The CR-DRWT is placed on a steel frame connected to the floor of the wind tunnel; see Fig. 3. For mounting, testing, and dismantling of the turbines, a time slot of 2 h was available. Wind speeds were increased in 1 $m\,s^{-1}$ increments from the moment the turbine self-started, starting at 4 $m\,s^{-1}$ up to a maximum of 15 $m\,s^{-1}$. The DC generator is connected to a programmable Chroma DC load. The resistance of the programmable load is increased at each wind speed until the maximum power point is found. The resistance, voltage, current, and power production are measured for 10 s with 0.1 s intervals. From the 100 data points per wind speed, average values and standard deviations are determined. The measured average power is then combined with the tunnel speed, air density, and rotor surface area to determine the power coefficient (CP) of the wind turbine.

2.3 BEM Model for dual-rotational armature

The BEM model in this study is based on the work of Amoretti et al. (2023), who developed a configurable BEM model for dual-rotor systems with two distinct rotors with individual generators. The present work extends this model: as in a dual-rotational armature configuration, both rotors are connected through a single generator. The model has the following assumptions: the flow is considered to be inviscid and incompressible, the system is in a stationary state, the retroaction from the second rotor to the first one is neglected, there is no radial speed taken into account, and the expansion of the flow at the rear of the first rotor is not considered. The last assumption is made because the expansion of two adjacent concentric annular sections would result in the intersection of the two respective flows and give complex flow velocity calculations (Amoretti et al., 2023). The model and the proposed extensions to it are presented in the following sections.

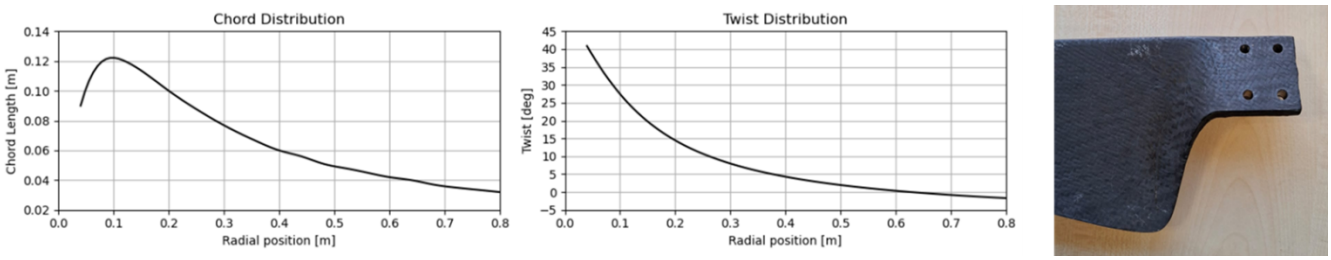

Figure 2. Aerodynamic design of both rotors of the DRWT. Left: the chord distribution. Middle: the twist distribution. Right: zoom-in on the root section of the blades.

Figure 3. The CR-DRWT in the wind tunnel at CSTB.

2.3.1 Single-rotor BEM

For this study, the definition of rotor, blade, and blade elements is in accordance with what is shown in Fig. 4. A rotor with radius R_{rotor} and hub radius R_{hub} rotates at angular velocity Ω about the axial direction $\overrightarrow{e_x}$. Each blade is discretized into N elements of length $\mathrm{d}r$ at radial position r, characterized by chord length c, twist angle β, and the aerodynamic profile.

The axial and tangential forces on a blade element are then as in Eqs. (1) and (2):

$$\mathrm{d}F_x = \frac{1}{2}\cdot\rho\cdot c\cdot \mathrm{d}r\cdot V_{\text{br}}^2\cdot\Big[C_{\text{L}}\cdot\cos(\Phi) + C_{\text{D}}\cdot\sin(\Phi)\Big], \tag{1}$$

$$\mathrm{d}F_\theta = \frac{1}{2}\cdot\rho\cdot c\cdot \mathrm{d}r\cdot V_{\text{br}}^2\cdot\Big[C_{\text{L}}\cdot\sin(\Phi) - C_{\text{D}}\cdot\cos(\Phi)\Big], \tag{2}$$

where ρ is the air density; V_{br} is the relative velocity seen by the blade; C_{L} and C_{D} are the airfoil lift and drag coefficients; and Φ is the sum of the angle of attack α, pitch angle, and twist angle β. The torque produced by a blade element is described as in Eq. (3), leading to a total rotor power as in Eq. (4), in which B is the number of blades of the turbine. The power coefficient (C_{p}) can be determined as in Eq. (5), where V_{ax0} is the upstream wind speed.

$$\mathrm{d}M = r\cdot\mathrm{d}F_\theta \tag{3}$$

$$P_{\text{turbine}} = B\cdot\int_{R_{\text{rotor}}}^{R_{\text{hub}}}\Omega\cdot\mathrm{d}M \tag{4}$$

$$C_{\text{p}} = \frac{P_{\text{turbine}}}{P_{\text{wind}}} = \frac{P_{\text{turbine}}}{\left[\frac{1}{2}\cdot\rho\cdot\pi\cdot {R_{\text{rotor}}}^2\cdot {V_{\text{ax0}}}^3\right]} \tag{5}$$

The axial and tangential velocities seen by the blade are modified by the induction coefficients a and a', leading to the relative velocity following Eq. (8).

$$V_{\text{bax}} = (1-a)\cdot V_{\text{ax0}} \tag{6}$$

$$V_{\text{bt}} = \left(1+a'\right)\cdot\Omega\cdot r \tag{7}$$

$$V_{\text{br}} = \sqrt{V_{\text{bax}}^2 + V_{\text{bt}}^2} \tag{8}$$

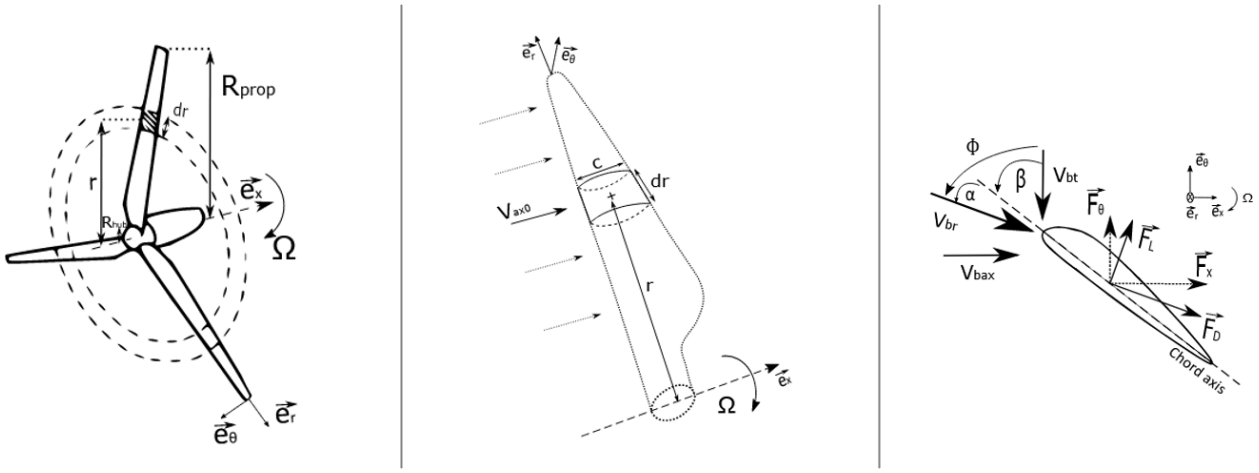

Figure 4. BEM parameter definition. Left: global wind turbine; middle: blade element definition; right: flow velocities and forces seen by a blade element. Adapted from Figs. 2 to 4 from Amoretti et al. (2023).

The induction coefficients are computed iteratively via a fixed-point algorithm presented in Amoretti et al. (2023), and, for each iteration, the coefficients are calculated using Eqs. (9) and (10). The iterative convergence criterion is set to $\varepsilon = 10^{-3}$.

$$a_{(n+1)} = \frac{1}{\frac{4 \cdot F \cdot \sin(\Phi)^2}{s \cdot [C_L \cdot \cos(\Phi) + C_D \cdot \sin(\Phi)]} - 1} \tag{9}$$

$$a'_{(n+1)} = \frac{1}{\frac{4 \cdot F \cdot \sin(\Phi) \cdot \cos(\Phi)}{s \cdot [C_L \cdot \sin(\Phi) - C_D \cdot \cos(\Phi)]} - 1} \tag{10}$$

In the above, s is the local solidity shown in Eq. (11), and F is Prandtl's tip loss factor (Hansen, 2015), as in Eqs. (12) and (13):

$$s = \frac{c \cdot B}{2 \cdot \pi \cdot r}, \tag{11}$$

$$\mathrm{F} = \frac{2}{\pi} \cdot \arccos\left(e^{-f}\right), \tag{12}$$

$$f = \frac{B}{2} \cdot \frac{R_{\mathrm{rotor}} - r}{r \cdot \sin(\Phi)}. \tag{13}$$

For high induction factors ($a > 0.2$), Spera's correction is applied (Hansen, 2015), and Eq. (9) is replaced by the following:

$$a_{(n+1)} = \frac{1}{2} \cdot \left[2 + K \cdot (1 - 2a) - \sqrt{(K(1-2a)+2)^2 + 4\left(K \cdot a^2 - 1\right)}\right], \tag{14}$$

with

$$K = \frac{4 \cdot F \cdot \sin(\Phi)^2}{s \cdot [C_L \cdot \cos(\Phi) + C_D \cdot \sin(\Phi)]}. \tag{15}$$

2.3.2 Wake velocity evolution

For the second rotor, the axial and tangential velocities downstream of the upstream rotor evolve with the distance after the rotor. The velocity evolution is defined with a distance coefficient $C_{\mathrm{distance}}(x)$ based on propeller stages (Gur, 2019), in which x is the distance from the first rotor.

$$C_{\mathrm{distance}}(x) = 1 + \frac{x}{\sqrt{x^2 + {R_{\mathrm{rotor}}}^2}} \tag{16}$$

The wake velocities at distance x from the rotor are then calculated as follows:

$$V_{\mathrm{ax}}(x) = V_{\mathrm{ax0}} \cdot (1 - C_{\mathrm{distance}}(x) \cdot a), \tag{17}$$

$$V_{\mathrm{t}}(x) = -a' \cdot \Omega \cdot r \cdot C_{\mathrm{distance}}(x). \tag{18}$$

2.3.3 Dual-rotor configuration

For the second rotor at distance $x = d$ downstream from the upstream rotor, the upstream wind velocities are now $V_{\mathrm{ax}}(d)$ and $V_{\mathrm{t}}(d)$. The axial velocity seen by the second rotor blade is calculated using Eq. (19). The tangential velocity depends on rotation direction – in this case, the counter-rotating configuration, thus following Eq. (20).

$$V_{\mathrm{bax2}} = (1 - a_2) \cdot V_{\mathrm{ax}}(d) \tag{19}$$

$$V_{\mathrm{bt2}} = \left(1 + a'_2\right) \cdot (\Omega_2 \cdot r - V_{\mathrm{t}}(d)) \tag{20}$$

The BEM algorithm is applied to both rotors sequentially, with the downwind rotor calculation incorporating modified inflow conditions. All other BEM equations (forces, induction factors, corrections) remain structurally identical for the second rotor. The model accepts geometrical parameters (blade geometry, rotor radii, number of blades), aerodynamic data (lift–drag polars), operational parameters (rotational speeds), environmental conditions (wind speed, air density), and configuration settings (rotor spacing, rotation direction).

2.3.4 Extension to the model for dual-rotational armature design

In order for a CR-DRWT with a dual-rotational armature design to be in balance, both rotor torques need to be equal (Kutt et al., 2020; Li et al., 2021). For a range of prescribed tip speed ratios of the upstream rotor, valid operating tip speed ratios of the downstream rotor are determined by enforcing a torque balance condition under the wake induced by the upstream rotor. The procedure used to determine these torque-balanced operating points is described in Table 1.

The output is a list of operating points where the system is in balance according to Eq. (22). Throughout the algorithm shown in Table 1, a tolerance for torque balance of 0.05 Nm is given in order to find possible solutions. For each point of balance, the net generator RPM is the sum of the RPM of both rotors as the system is counter-rotating, as shown in Eq. (21). The power then follows Eq. (23), and the power coefficient of the CR-DRWT is according to Eq. (24), where P_{wind} is calculated as in Eq. (5).

$$\Omega_{\text{generator}} = \Omega_{\text{upstream rotor}} + \Omega_{\text{downstream rotor}} \tag{21}$$

$$T_{\text{CR-DRWT}} = T_{\text{upstream rotor}} = T_{\text{downstream rotor}} \tag{22}$$

$$P_{\text{CR-DRWT}} = \left(\Omega_{\text{generator}} \cdot T_{\text{CR-DRWT}}\right) \tag{23}$$

$$C_{\text{p\_total}} = \frac{P_{\text{CR-DRWT}}}{P_{\text{wind}}} \tag{24}$$

2.4 Optimization of extended CR-DRWT BEM model

The ISWTC competition of 2025 included a Weibull distribution ($A = 7.1$ and $k = 2.4$) to calculate the annual energy production (AEP). Thereto, the turbine is optimized for performance under these conditions. A sweep optimization strategy to identify the pitch angle combination that maximizes the annual energy production (AEP) of the dual-rotor wind turbine is employed. The upstream and downstream rotor pitch angles are each varied independently across a grid from 0 to 10° in steps of 1°, yielding 121 unique pitch combinations to be evaluated in full. For each combination, the aerodynamic performance is computed across a range of wind speeds from 4 to 15 m s^{-1}, with a 1 m s^{-1} interval, using the extended BEM model. For each wind speed, only the operating point yielding the highest overall power output is selected. The AEP for each pitch combination is then calculated using the Weibull parameters. The pitch combination producing the highest total AEP across all wind speeds is then identified as the global optimum. Finally, the BEM will then be simulated with the theoretically optimal pitch and tip speed ratio (TSR) settings to assess the maximum performance of the CR-DRWT. This will then be compared to the wind tunnel measurements as well.

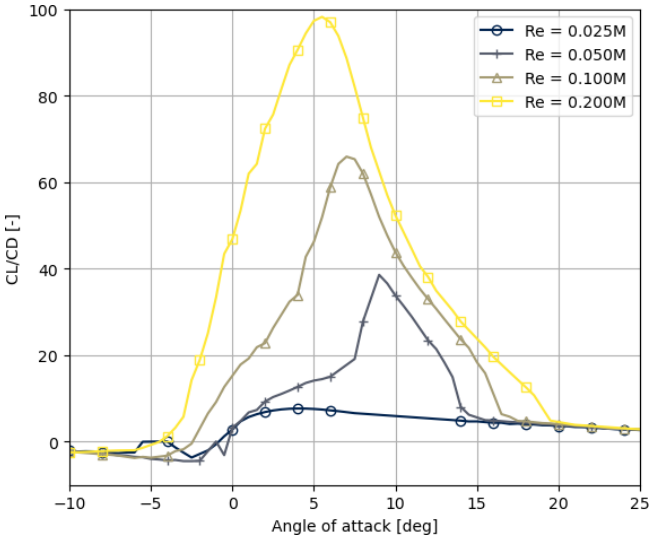

Figure 5. Profile aerodynamics of SG6043 airfoil at $N_{\text{crit}} = 9$.

3 Results

This chapter present the results of the wind tunnel test and BEM model, including optimization. First, the results of the wind tunnel are presented together with the BEM model validation.

3.1 Airfoil data

The aerodynamic data to describe the airfoil performances were generated with the 2D airfoil solver XFoil in QBlade (QBlade, 2026; Drela, 1989). Lift and drag coefficients for angles of attack from −10 to 25° are calculated with a transition amplification ratio of $N_{\text{crit}} = 9$, corresponding to clean wind tunnel conditions. Figure 5 displays the aerodynamic data. The curve is then extrapolated to 360° (Montgomerie, 2004). For the BEM code, the aerodynamic data are interpolated according to the individual Reynolds number for each blade element.

3.2 Wind tunnel test

Air pressure in the wind tunnel at the time of the experiment was 1018 hPa, average humidity was 51.2 %, and average temperature was 25.5 °C. The density is then calculated to be 1.18 kg m^{-3}. The wind tunnel speed is determined through the measurement of the dynamic pressure and air density. Rotor RPM was measured in 10 RPM increments. The data were acquired through a laptop interface connected with the turbine, and measurements were sampled at discrete wind speed intervals rather than being continuously logged due to the streaming nature of the sensor output. The generator RPM is determined through the voltage and current measurements, as well as the generator characteristics. At 6 m s^{-1}, optimal operational pitch settings were determined

Table 1. Algorithm to determine balance torque of CR-DRWT.

Algorithm torque balance CR-DRWT:

for each wind speed:
  for each prescribed front rotor tip speed ratio:
  Compute the aerodynamic torque and rotational speed of the upstream rotor
  Compute the wake conditions at the downstream rotor plane induced by the upstream rotor
  Fix the wake conditions and evaluate the downstream rotor torque over a predefined range of rear rotor tip speed ratios
  Identify all intervals where the downstream rotor torque crosses the upstream rotor torque
  for each identified sign change interval:
  Apply bisection to find the downstream rotor tip speed ratio at which both torques are balanced
  Compute the downstream rotor rotational speed and power output
  Compute the total system power
  Store the torque balanced operating point
  end for
  end for
end for

Output: torque-balanced operating points and power values for all wind speeds

by manually changing the pitch angles and resistance values of the DC load to reach maximum power production. The settings for the collective pitch angles were 8.6° for the upstream rotor and 1.7° for the downstream rotor throughout the experiment. The results for the wind tunnel test are presented in Table 2. The turbine self-starts around $3.5\,\mathrm{m\,s^{-1}}$ and starts producing power at $4\,\mathrm{m\,s^{-1}}$. A startup procedure is developed where the downstream rotor is allowed to operate first by breaking the upstream rotor and consecutively allowing the upstream rotor to start only once the downwind rotor reached an operating point. Power, voltage, and current output are measured for 10 s with a 0.1 s sampling rate. Mean values are calculated, as well as the standard deviation. Maximum power production was 1013.79 ± 8.58 W at $15.00\,\mathrm{m\,s^{-1}}$ wind tunnel speed. The maximum RPM of the generator was 2150 RPM. The rear rotor was generally rotating slower than the front rotor at lower wind speeds, while, at higher wind speeds, the RPM became more similar for both rotors, and the rear rotor seemed to stabilize. Net generator RPM did keep increasing with wind speed.

A simulation using the BEM code from Sect. 2.3, with identical inputs for pitch during the experiment, has been performed. The corresponding pair of rotational speeds where torque balance is present and which are closest in power output to the measurement is selected. The results for the power production, the CP, and RPMs are shown in Figs. 6, 7, and 8, together with the CSTB wind tunnel results. The BEM code imposes a 70 %–90 % electrical efficiency of the generator on the aerodynamic power. This efficiency of the generator has been determined for similar operational conditions in previous studies (Adema et al., 2025; Jansma, 2024). The CP values for the downstream rotor are calculated with the reduced wind speed after the upstream rotor following Eq. (17).

Overall, the BEM model follows the outcome of the wind tunnel tests well with respect to power output and CP values. Both rotors operate at similar CP values. However, the modelled RPM values start to deviate from around $11\,\mathrm{m\,s^{-1}}$ onwards. The measurements show a stable upstream rotor RPM of 1050, but the model requires a faster rotating upstream rotor to enforce torque balance at that power point. The model, however, does follow the operational RPM of the generator, indicating that the inferred RPM values from the generator characteristic were correct. The discussion in the next section further elaborates on the observed deviation in RPM measurements.

3.3 Optimization

The results of the optimization sweep are presented in Fig. 9. The plot shows the cumulative results of 121 pairs of pitch combinations. The optimization favours when the upstream rotor operates at a high pitch angle and when the downstream rotor operates at a low pitch angle. The best configuration is an upstream rotor at pitch 9° and a downstream rotor at 0°, yielding a possible AEP of 2150 kWh. The results of the extended BEM model with the optimized pitch settings are shown in Figs. 10 and 11. The maximum aerodynamic power output of the CR-DRWT at $15\,\mathrm{m\,s^{-1}}$ is 2251 W, with a maximum CP of 0.56 at 14 and $15\,\mathrm{m\,s^{-1}}$. This maximum aerodynamic power is above the rated capacity of 1400 W of the current generator. The corresponding TSR values are calculated using the free-stream wind speed for the upstream rotor and the reduced axial velocity for the downstream rotor. The mean TSR values across the wind speed range for the upstream and downstream rotor are 3.2 and 6.6, respectively, leading to a maximum RPM of the generator at $15\,\mathrm{m\,s^{-1}}$ of 1603 RPM, which is significantly below the measured 2150 RPM in the wind tunnel test at the same wind speed. Compared to the wind tunnel tests at CSTB, the optimized CR-DRWT could outperform the current turbine. The cur-

Table 2. Measurement results from CSTB wind tunnel tests.

Wind tunnel speed [m s^{-1}]	Voltage [V]	Current [A]	Power [W]	CP [–]	Downstream rotor [RPM]	Upstream rotor [RPM]	Generator [RPM]
4.14	22.71 ± 0.54	0.42 ± 0.01	9.49 ± 1.63	0.11 ± 0.02	60	340	400
5.27	31.57 ± 0.33	1.05 ± 0.01	33.31 ± 4.00	0.19 ± 0.02	260	390	650
5.90	39.38 ± 0.29	1.43 ± 0.03	56.33 ± 1.61	0.23 ± 0.01	250	540	790
7.10	38.38 ± 0.05	3.48 ± 0.01	133.58 ± 1.27	0.32 ± 0.00	210	630	840
8.16	41.75 ± 0.22	5.01 ± 0.02	209.25 ± 1.99	0.33 ± 0.00	245	705	950
9.14	49.86 ± 0.22	6.04 ± 0.01	301.05 ± 2.20	0.33 ± 0.00	360	830	1190
10.05	57.54 ± 0.19	6.97 ± 0.01	401.31 ± 1.50	0.33 ± 0.00	400	940	1340
11.15	66.45 ± 0.15	8.07 ± 0.05	535.91 ± 3.40	0.33 ± 0.00	520	1000	1520
12.18	73.51 ± 0.23	8.91 ± 0.07	654.75 ± 5.59	0.31 ± 0.00	620	1050	1670
13.04	80.12 ± 0.22	9.74 ± 0.07	780.29 ± 5.54	0.30 ± 0.00	800	1050	1850
13.93	85.91 ± 0.32	10.37 ± 0.08	890.98 ± 5.54	0.28 ± 0.00	960	1050	2010
15.00	91.72 ± 0.31	11.05 ± 0.07	1013.79 ± 8.58	0.25 ± 0.00	1100	1050	2150

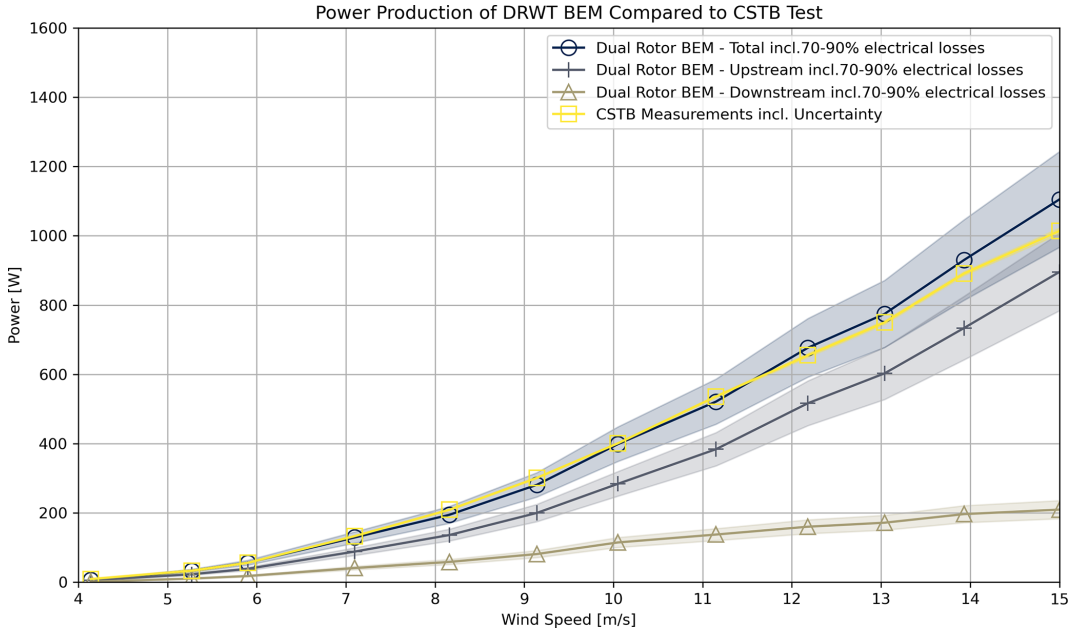

Figure 6. Results of power production during the wind tunnel test compared to BEM results. The figure shows both rotors individually, the CR-DRWT, and the wind tunnel test data.

rent plots show only aerodynamic performance. However, even including 70 %–90 % electrical losses, the optimized turbine outperforms the current measurements. Also, Fig. 11 shows that the optimization maximizes the performance of the downstream rotor, with a much higher CP for the downstream rotor for all wind speeds compared to the CP for the upstream rotor.

4 Discussion

The current iteration of the CR-DRWT shows improvement with respect to earlier work (Adema et al., 2025), especially as precise RPM and pitch measurements are performed. Absolute CP values of around 0.5 are found in both field studies and modelling of CR-DRWT systems (Amoretti et al., 2023; Jung et al., 2005; Koehuan et al., 2017). The current experimental results reach a maximum CP of only 0.33. The findings of this study are more in line with earlier wind tunnel experiments on a CR-DRWT of comparable size (Mitulet et al., 2015; Zhao et al., 2020). There is therefore still potential to increase the efficiency of turbines with limited rotor size. The optimization does show theoretical values reaching a CP of 0.56, confirming the possible improvements.

While the extended BEM model follows the experiment measurements well, the deviation between the modelled and measured upstream rotor RPM values above 11 m s^{-1} war-

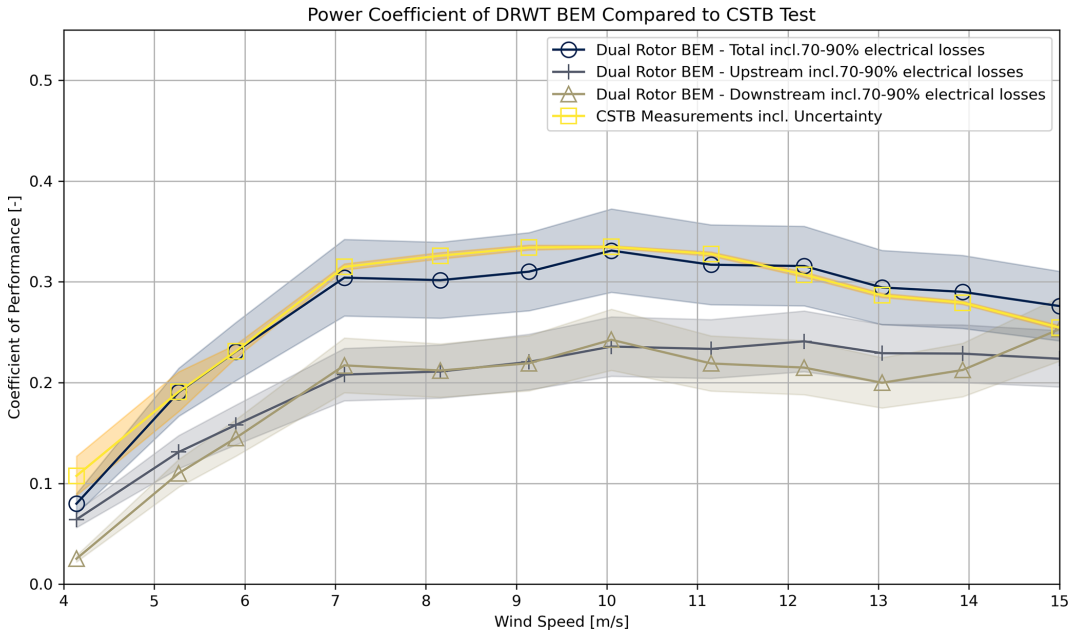

Figure 7. Results of the coefficient of performance during the wind tunnel test compared to BEM results. The figure shows both rotors individually, the CR-DRWT, and the wind tunnel test data.

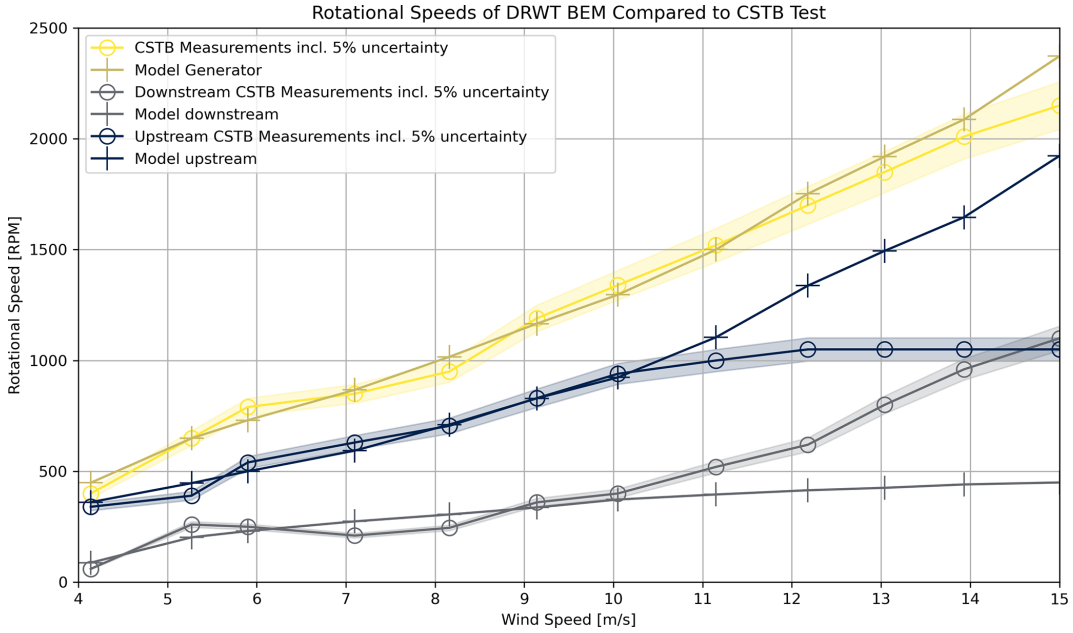

Figure 8. Results of rotational speeds during the wind tunnel test compared to BEM results. The figure shows both rotors individually, the CR-DRWT, and the wind tunnel test data.

rants further consideration. The experimental measurements at the upstream rotor plateau at approximately 1050 RPM, and the model predicts a continuously increasing RPM to keep torque balance. A possible explanation lies in the measurement system employed during the wind tunnel campaign. The upstream rotor RPM was measured using a light gate sensor reading optical pulses through a slotted disc. It is suspected that a limitation in the pulse-counting implementation code effectively imposed an artificial ceiling on the recorded RPM values. This would cause the sensor output to remain at a fixed reading even as the true rotational speed continued to increase. The generator RPM, derived from the generator characteristic curve, is therefore considered to be the more reliable indicator of actual generator RPM. This interpreta-

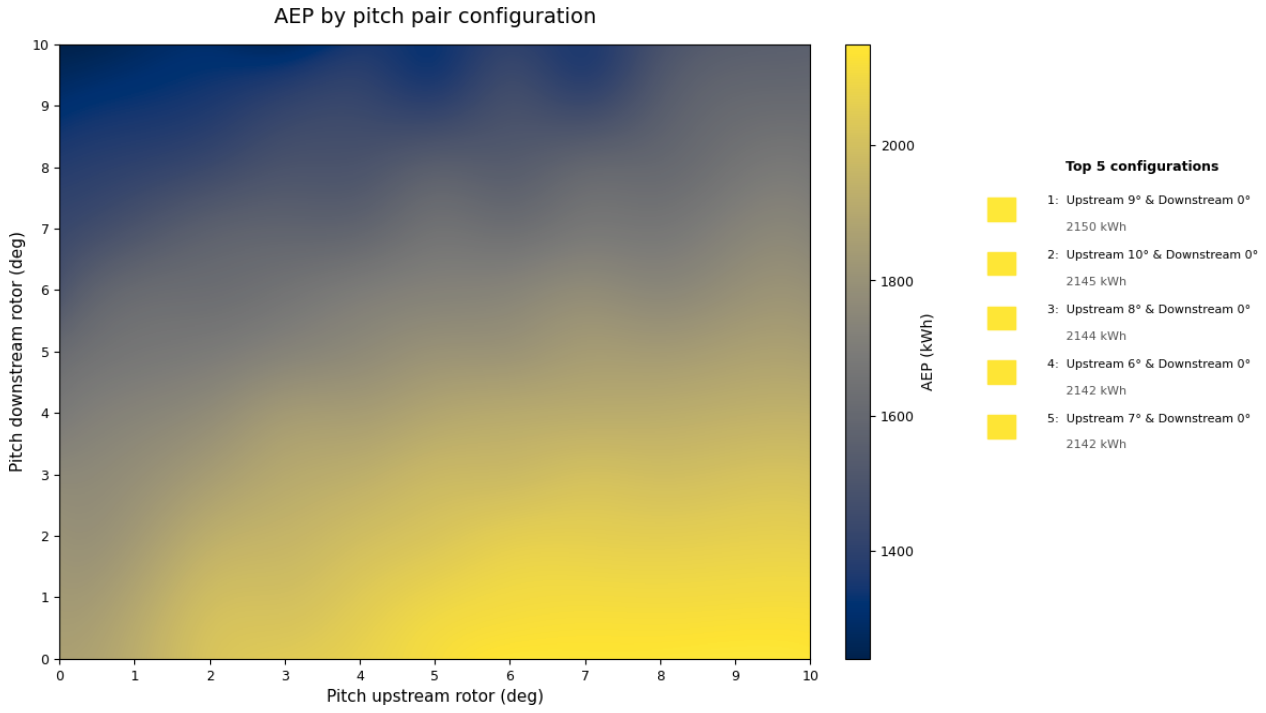

Figure 9. Results of optimization.

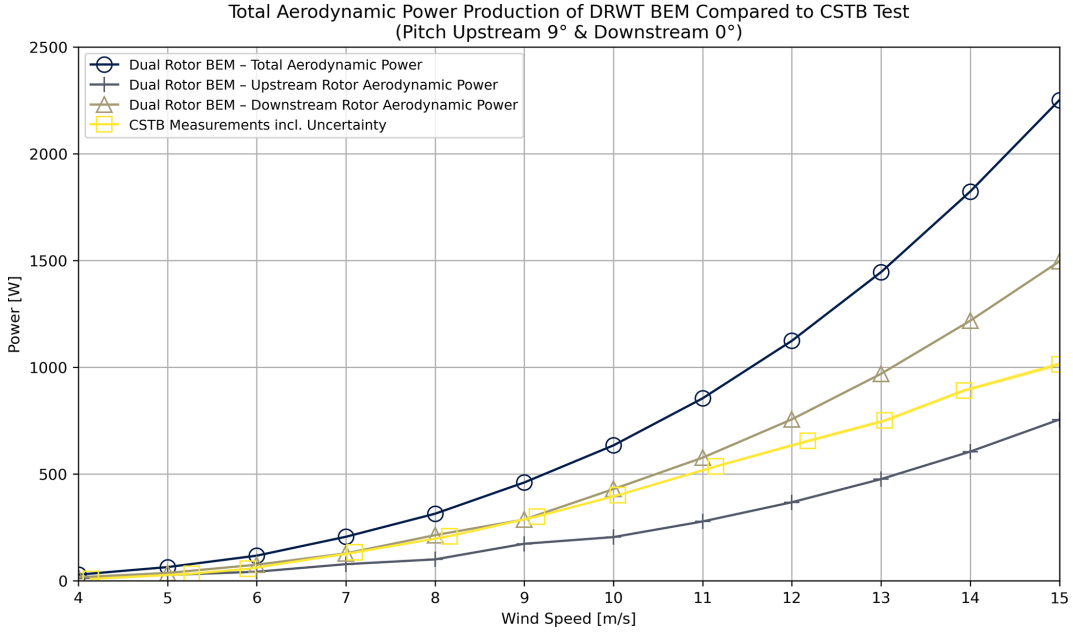

Figure 10. Power production of optimized CR-DRWT.

tion is further supported by the fact that the total generator RPM coming from the BEM model matches well with the derived generator RPM.

The theoretical optimization shows the downstream rotor operating with high CP values and limiting the upstream rotor efficiency. This raises questions about if a single rotor could achieve better AEP performance than the optimized CR-DRWT. Thereto, the BEM model is run with an isolated upstream rotor, effectively modelling single-rotor operation, and the optimal operation point is found by sweeping across a range of pitch angles and TSR values and maximizing AEP. The optimal aerodynamic performance of a single rotor is

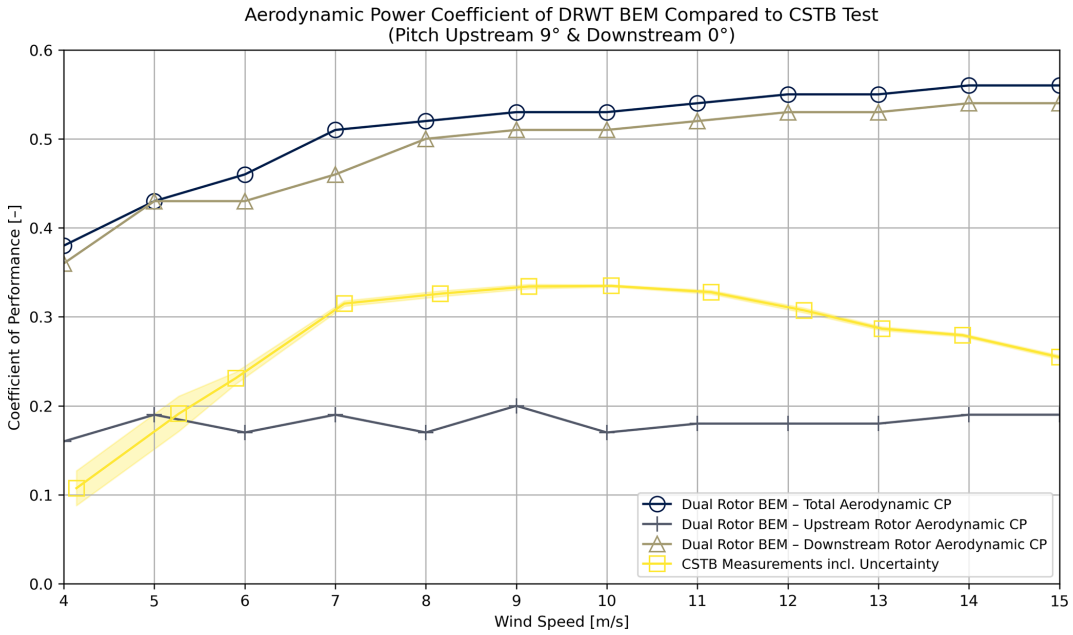

Figure 11. Power coefficient of optimized CR-DRWT.

found at 0° pitch and a TSR of 6.5. The results are shown in Fig. 10. A single rotor can reach equally good power and efficiency. The CR-DRWT has slightly higher AEP with 2322 kWh compared to 2093 kWh for the single rotor. However, the operational point of both systems is different, with the CR-DRWT reaching maximum power at 1603 RPM at the generator and 1164 RPM for the single rotor, highlighting that, for both configurations, a different generator is likely needed to reach optimal operation. What is worth mentioning is that Adema et al. (2025) concluded that the current direct-drive configuration is not optimized for single-rotor operation. The same turbine with 2.5° pitch for the upstream rotor and a stationary downstream rotor only reached a maximum CP in single-rotor operation of 0.23. For the current small wind turbine generator, the additional costs for a second rotor may be lower than those for the addition of a gearbox, highlighting the potential of DRWT systems in compact simplified designs (Booker et al., 2010).

In most existing wind tunnel experiments, Reynolds numbers are much lower than those encountered in actual situations, limiting their ability to replicate real-world conditions. This limits the ability to model and predict the performance of DRWT's under real-world conditions (Hollands et al., 2020). The same holds for the current experiment with Reynolds numbers between 25 000 and 200 000. Attention needs to be paid to possible inaccuracies in predicting airfoil characteristics at such low numbers.

An attempt to use a BEM model incorporating both axial and tangential influences on the inflow at the downstream rotor (Amoretti et al., 2023), as well as an extension for a dual-rotational armature design, has shown good agreement with the current findings, though some deviations remain. An additional CFD analysis of the current turbine configuration presented in this study will be a valuable addition in understanding the flow field around both rotors. Knowing the detailed flow field around the downstream rotor, a detailed aerodynamic design can be performed to further optimize the CR-DRWT. Also, such an analysis may reveal unknown (three-dimensional) aerodynamic effects not captured in current BEM model.

Finally, calculation methods have been proposed for optimizing the downstream rotor geometry for DRWT designs (Bontempo and Manna, 2025; Wang et al., 2018). Currently, for simplicity, the downstream rotor is mirrored with respect to the upstream rotor. Using the BEM model presented in this work, a detailed blade design using these design methods can be performed to further increase the performance of dual-rotor wind turbines.

5 Conclusions

This study investigates the performance of a CR-DRWT with a dual-rotational armature configuration through wind tunnel testing at CSTB in Nantes, France. The research extends previous work by incorporating enhanced measurement capabilities including RPM and pitch angle sensors, the development of an extended BEM model for dual-rotational armature systems, and implementation of a sweep optimization strategy to identify optimal operating parameters. Wind tunnel tests were conducted at wind speeds ranging from 4 to 15 m s^{-1}, with a 1.6 m diameter rotor and two rotors with 0.39 D spacing. The CR-DRWT achieved a maximum power

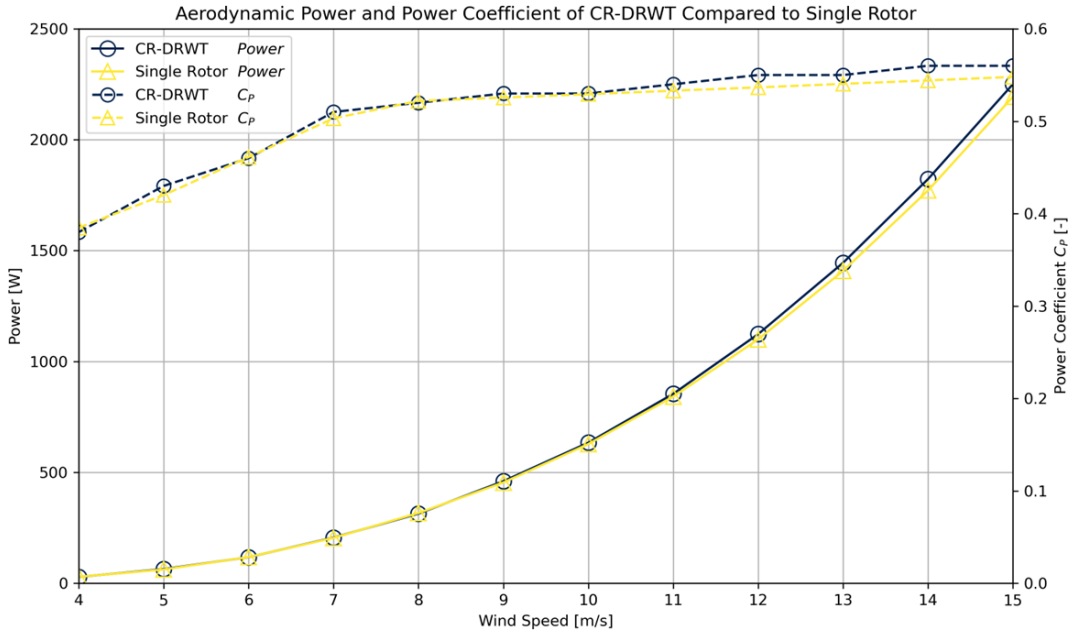

Figure 12. Comparison between theoretical optimal power production and power coefficient of CR-DRWT and single rotor.

output of 1014 W. The extended BEM model is validated against experimental data. The main conclusions are outlined below.

The extended BEM mode for dual-rotational armature design showed good overall agreement with wind tunnel measurements for power production, efficiency, and generator RPM, and an optimization strategy revealed optimum operational parameters. The upstream rotor RPM measured by the light gate sensor was limited at approximately 1050 RPM above 11 m s^{-1}, likely due to a pulse-counting limitation in the data acquisition code, as the derived generator RPM continued to rise, in line with model predictions across the full wind speed range.

Experimental wind tunnel testing achieved a maximum CP of 0.33, which is higher than previous iterations of the same turbine but below the theoretically optimized value of 0.56, indicating substantial room for improvement through optimal pitch angle, tip speed ratios for both rotors, and generator choice or redesign.

The sweep optimization identified an upstream rotor pitch of 9° and downstream rotor pitch of 0° as the optimal configuration for this CR-DRWT, with a theoretical AEP of 2150 kWh. The optimization consistently favoured a high-efficiency downstream rotor operation at high CP values, while the upstream rotor operates with reduced efficiency, indicating that shared power production across both rotors is essential for maximizing overall system performance.

The CR-DRWT with dual-rotational armature design demonstrated reliable operation with self-starting capability at 3.5 m s^{-1}. The dual-rotational armature configuration eliminates the need for gearboxes, potentially offering a more cost-effective and mechanically simpler solution for compact small wind turbine designs, particularly suited for urban applications requiring low noise and vibration.

To advance the understanding and performance of CR-DRWT systems, detailed computational fluid dynamics simulations should be performed to capture 3D flow effects not modelled by the current BEM approach. Experiments at higher Reynolds numbers closer to real-world operational conditions are needed to improve performance prediction accuracy and to validate airfoil characteristics. The development of blade geometries specifically optimized for the downstream rotor, rather than using mirrored configurations, should be pursued using the validated BEM model and advanced design methods from the recent literature. Field testing under real atmospheric conditions is essential to assess the practical performance, durability, and economic viability of the optimized CR-DRWT configuration.

Code and data availability. The models and data used in this paper can be requested from the corresponding author upon request.

Author contributions. NA: conceptualization, formal analysis, writing (original draft preparation). JGV: investigation, resources, writing (original draft preparation). WS: investigation, resources, writing (review and editing). AdR: funding acquisition, supervision, writing (review and editing). GS: writing (review and editing).

Competing interests. The contact author has declared that none of the authors has any competing interests.

Acknowledgements. The authors of this paper would like to express their sincere gratitude to Callum Morgan, Sjoerd Kluvers, Wessel Smeenge, Bram Roorda, and Marijn Verbeek, who helped design and build the current iteration of the turbine used in this work; their efforts cannot go unmentioned. Second, the staff at CSTB is thanked for their assistance and guidance during the wind tunnel measurements. Finally, the authors would like to thank Caroline Braud for her effort in facilitating the hosting of the ISWTC at CSTB in 2025.

Financial support. This research has been supported by the Nationaal Regieorgaan Praktijkgericht Onderzoek SIA (grant no. RAAK.MKB17.007).

Review statement. This paper was edited by Jonathan Whale and reviewed by two anonymous referees.

References

Adema, N., Swart-Ranshuysen, W., De Ruijter, A., and Schepers, G.: Wind Tunnel Test of Counter-Rotating Dual Rotor Wind Turbine With Double Rotational Armature Design, Wind Energy, 28, https://doi.org/10.1002/we.70039, 2025.

Al-Obaidi, A. S. M. and Madivaanan, G.: Investigation of the Blockage Correction to Improve the Accuracy of Taylor's Low-Speed Wind Tunnel, J. Phys. Conf. Ser., 2222, 012008, https://doi.org/10.1088/1742-6596/2222/1/012008, 2022.

Amoretti, T., Huet, F., Garambois, P., and Roucoules, L.: Configurable dual rotor wind turbine model based on BEM method: Co-rotating and counter-rotating comparison, Energ. Convers. Manage., 293, 117461, https://doi.org/10.1016/j.enconman.2023.117461, 2023.

Bai, H., Wang, N., and Wan, D.: Numerical study of aerodynamic performance of horizontal axis dual-rotor wind turbine under atmospheric boundary layers, Ocean Eng., 280, 114944, https://doi.org/10.1016/j.oceaneng.2023.114944, 2023.

Bereziartua-Gonzalez, L., Retegi, A., and Ukar, O.: Human-centered integration of small wind turbines in urban environments: a semi-systematic review from an industrial design perspective, Front. Sustain. Cities, 7, https://doi.org/10.3389/frsc.2025.1561894, 2025.

Bianchini, A., Bangga, G., Baring-Gould, I., Croce, A., Cruz, J. I., Damiani, R., Erfort, G., Simao Ferreira, C., Infield, D., Nayeri, C. N., Pechlivanoglou, G., Runacres, M., Schepers, G., Summerville, B., Wood, D., and Orrell, A.: Current status and grand challenges for small wind turbine technology, Wind Energ. Sci., 7, 2003–2037, https://doi.org/10.5194/wes-7-2003-2022, 2022.

Bontempo, R. and Manna, M.: Optimum design of contra-rotating wind turbines with adjacent rotors, Energ. Conv. Manage., 324, 119267, https://doi.org/10.1016/j.enconman.2024.119267, 2025.

Booker, J. D., Mellor, P. H., Wrobel, R., and Drury, D.: A compact, high efficiency contra-rotating generator suitable for wind turbines in the urban environment, Renew. Energ., 35, 2027–2033, https://doi.org/10.1016/j.renene.2010.02.003, 2010.

Braud, C., Podvin, B., and Deparday, J.: Study of the wall pressure variations on the stall inception of a thick cambered profile at high Reynolds number, Phys. Rev. Fluids, 9, 014605, https://doi.org/10.1103/PhysRevFluids.9.014605, 2024.

Calautit, K. and Johnstone, C.: State-of-the-art review of micro to small-scale wind energy harvesting technologies for building integration, Energ. Conv. Manage., 20, 100457, https://doi.org/10.1016/j.ecmx.2023.100457, 2023.

Chagas, C. C. M., Pereira, M. G., Rosa, L. P., da Silva, N. F., Freitas, M. A. V., and Hunt, J. D.: From Megawatts to Kilowatts: A Review of Small Wind Turbine Applications, Lessons From The US to Brazil, Sustainability, 12, 2760, https://doi.org/10.3390/su12072760, 2020.

Chen, T. Y. and Liou, L. R.: Blockage corrections in wind tunnel tests of small horizontal-axis wind turbines, Exp. Therm. Fluid Sci., 35, 565–569, https://doi.org/10.1016/j.expthermflusci.2010.12.005, 2011.

Drela, M.: XFOIL: An Analysis and Design System for Low Reynolds Number Airfoils, in: Low Reynolds Number Aerodynamics, 1–12, https://doi.org/10.1007/978-3-642-84010-4_1, 1989.

Erturk, E., Sivrioglu, S., and Bolat, F. C.: Analysis Model of a Small Scale Counter-Rotating Dual Rotor Wind Turbine with Double Rotational Generator Armature, International Journal of Renewable Energy Research (IJRER), 8, 1849–1858, 2018.

Gur, O.: Extending Blade-Element Model to Contra-Rotating Configuration, IOP Conf. Ser., Mater. Sci. Eng., 638, 012001, https://doi.org/10.1088/1757-899X/638/1/012001, 2019.

Habash, R. W. Y., Groza, V., Yang, Y., Blouin, C., and Guillemette, P.: Performance of a Contrarotating Small Wind Energy Converter, International Scholarly Research Notices, 2011, 828739, https://doi.org/10.5402/2011/828739, 2011.

Hansen, M.: Aerodynamics of Wind Turbines, 3rd Edn., Routledge, London, 188 pp., https://doi.org/10.4324/9781315769981, 2015.

Hollands, E. O., He, C., and Gan, L.: A particle image velocimetry study of dual-rotor counter-rotating wind turbine near wake, J. Vis., 23, 425–435, https://doi.org/10.1007/s12650-020-00643-0, 2020.

Jansma, H.: Development and Optimization of a Generator Test Rig for Small Wind Turbines: Improving Performance and Efficiency, MSc Thesis, Hanze UAS, Groningen, 74 pp., 2024.

Jeong, H., Lee, S., and Kwon, S.-D.: Blockage corrections for wind tunnel tests conducted on a Darrieus wind turbine, J. Wind Eng. Ind. Aerod., 179, 229–239, https://doi.org/10.1016/j.jweia.2018.06.002, 2018.

Jung, S. N., No, T.-S., and Ryu, K.-W.: Aerodynamic performance predictionof a 30 kW counter-rotating wind turbine system, Renew. Energ., 30, 631–644, https://doi.org/10.1016/j.renene.2004.07.005, 2005.

Jurasz, J., Bochenek, B., Wieczorek, J., Jaczewski, A., Kies, A., and Figurski, M.: Energy potential and economic vi-

ability of small-scale wind turbines, Energy, 322, 135608, https://doi.org/10.1016/j.energy.2025.135608, 2025.

Koehuan, V. A., Sugiyono, and Kamal, S.: Investigation of Counter-Rotating Wind Turbine Performance using Computational Fluid Dynamics Simulation, IOP Conf. Ser. Mater. Sci. Eng., 267, 012034, https://doi.org/10.1088/1757-899X/267/1/012034, 2017.

Kutt, F., Blecharz, K., and Karkosiński, D.: Axial-Flux Permanent-Magnet Dual-Rotor Generator for a Counter-Rotating Wind Turbine, Energies, 13, 2833, https://doi.org/10.3390/en13112833, 2020.

Lee, S., Kim, H., Son, E., and Lee, S.: Effects of design parameters on aerodynamic performance of a counter-rotating wind turbine, Renew. Energ., 42, 140–144, https://doi.org/10.1016/j.renene.2011.08.046, 2012.

Li, Y., Zhang, J., Li, Z., Yang, P., and Wang, H.: Design and verification of a novel double rotor without stator wind turbine generation system, Energy Reports, 7, 161–172, https://doi.org/10.1016/j.egyr.2021.10.041, 2021.

Mitulet, L.-A., Oprina, G., Chihaia, R.-A., Nicolaie, S., Nedelcu, A., and Popescu, M.: Wind Tunnel Testing for a New Experimental Model of Counter-rotating Wind Turbine, Procedia Engineer., 100, 1141–1149, https://doi.org/10.1016/j.proeng.2015.01.477, 2015.

Montgomerie, B.: Methods for Root Effects, Tip Effects and Extending the Angle of Attack Range to ±180°, with Application to Aerodynamics for Blades on Wind Turbines and Propellers, Swedish Defence Research Agency, https://www.foi.se/rest-api/report/FOI-R--1305--SE (last access: 3 June 2026), 2004.

Mühle, F., Adaramola, M. S., and Sætran, L.: The effect of rotational direction on the wake of a wind turbine rotor – a comparison study of aligned co- and counter rotating turbine arrays, Energy Proced., 137, 238–245, https://doi.org/10.1016/j.egypro.2017.10.346, 2017.

Newman, B. G.: Multiple actuator-disc theory for wind turbines,J. Wind Eng. Ind. Aerod., 24, 215–225, https://doi.org/10.1016/0167-6105(86)90023-1, 1986.

Ozbay, A., Tian, W., and Hu, H.: An Experimental Investigation on the Aeromechanics and Near Wake Characteristics of Dual-Rotor Wind Turbines (DRWTs), in: 32nd ASME Wind Energy Symposium, American Institute of Aeronautics and Astronautics, https://doi.org/10.2514/6.2014-1085, 2014.

Peng, X., Duan, L., Li, G., Jin, Y., and Han, Z.: Interference between main and auxiliary rotors in floating dual-rotor wind turbines under stationary and surge conditions, Ocean Eng., 322, 120462, https://doi.org/10.1016/j.oceaneng.2025.120462, 2025.

QBlade: QBlade – Next Generation Wind Turbine Simulation, https://qblade.org/, last access: 13 April 2026.

Rosenberg, A., Selvaraj, S., and Sharma, A.: A Novel Dual-Rotor Turbine for Increased Wind Energy Capture, J. Phys. Conf. Ser., 524, 012078, https://doi.org/10.1088/1742-6596/524/1/012078, 2014.

Schepers, J. G., Adema, N. C., Lipian, M., Kulak, M., Shahid, A., Best, A., Bendre, T., Gallicchio, I., Elsabbagh, A., Mostafa, A., Kim, T., Mikkelsen, R., Gaunaa, M., Teuwen, J. J. E., Rudolf, R. T., Wood, D., and Holierhoek, J. G.: Lessons learned from 10 years of wind tunnel tests on small wind turbines designed by students, J. Phys. Conf. Ser., 2767, 072009, https://doi.org/10.1088/1742-6596/2767/7/072009, 2024.

Simic, Z., Havelka, J. G., and Bozicevic Vrhovcak, M.: Small wind turbines – A unique segment of the wind power market, Renew. Energ., 50, 1027–1036, 2013.

Sundararaju, H., Lo, K. H., Metcalfe, R., and Wang, S. S.: Aerodynamics and CFD analysis of equal size dual-rotor wind turbine, J. Renew. Sustain. Ener., 9, 043305, https://doi.org/10.1063/1.4999500, 2017.

Wang, K., Liu, T., Wan, Y., Ong, M. C., and Wu, T.: Numerical Investigation on Aerodynamic Characteristics of Dual-Rotor Wind Turbines, J. Mar. Sci. Eng., 10, 1887, https://doi.org/10.3390/jmse10121887, 2022.

Wang, Z., Ozbay, A., Tian, W., and Hu, H.: An experimental study on the aerodynamic performances and wake characteristics of an innovative dual-rotor wind turbine, Energy, 147, 94–109, https://doi.org/10.1016/j.energy.2018.01.020, 2018.

Yin, F. F., Chen, J. J., Li, X. K., Ye, Z. L., Tang, W., Shen, X., and Guo, X. J.: A blade element momentum model for dual-rotor wind turbines considering inter-rotor velocity interferences, J. Phys. Conf. Ser., 2265, 042058, https://doi.org/10.1088/1742-6596/2265/4/042058, 2022.

Yuan, W., Tian, W., Ozbay, A., and Hu, H.: An experimental study on the effects of relative rotation direction on the wake interferences among tandem wind turbines, Sci. China Phys. Mech. Astron., 57, 935–949, https://doi.org/10.1007/s11433-014-5429-x, 2014.

Zhao, X., Zhou, P., Liang, X., and Gao, S.: The aerodynamic coupling design and wind tunnel test of contra-rotating wind turbines, Renew. Energ., 146, 1–8, https://doi.org/10.1016/j.renene.2019.06.118, 2020.